

**TOWARDS A MODEL BASED MEDICINE: A CLINICALLY MEANINGFUL  
APPROACH TO ILL-POSED INVERSE PROBLEMS IN QUANTITATIVE  
PHYSIOLOGY**

Sven Zenker \*

Jonathan Rubint†

Gilles Clermont \*

\* Center for Inflammation and Regenerative Modeling (CIRM) and the CRISMA Laboratory (Clinical Research, Investigation, and Systems Modeling of Acute illness) , Department of Critical Care Medicine, University of Pittsburgh School of Medicine, Pittsburgh, PA.

† Department of Mathematics, University of Pittsburgh, Pittsburgh, PA.

**Running Head:** Towards a model based medicine

**Word Count:** 5048

**Grant Support:** This research was partly funded by the National Heart, Lung and Blood Institute (R01-HL76157).

**Correspondence to:**

Gilles Clermont, MD, CM  
606 Scaife Hall  
CIRM and the CRISMA Laboratory  
Critical Care Medicine  
University of Pittsburgh  
3550 Terrace Street  
Pittsburgh, PA 15261

Tel: (412) 647 7980

Fax: (412) 647 3791

Email: cler@pitt.edu

## ABSTRACT

We model the diagnostic process in medicine as a map that iterates the probability density function (PDF) on a combined state/parameter space  $X$  of a mechanistic physiological model. This map incorporates a PDF on an observation space  $Y$ , which can be based on a population-level prior or on updates of such a prior, as well as patient-specific measurements with stochastic characteristics reflecting measurement uncertainty. Using a simple differential equation model of cardiovascular physiology, and a typical differential diagnostic situation (hypotension, fluid challenge) as an example, we show in simplified 2- and 3-dimensional simulation settings that a) even assuming uniform priors on  $X$ , multimodal PDFs are induced, their peaks corresponding to differential diagnoses, and b) the methodology in principle allows the assimilation of observations of both static conditions and dynamic responses into a quantitative assessment of patient status. Implications for our theoretical understanding of the differential diagnostic process in medicine and for practical quantitative medical decision making, incorporating mechanistic knowledge, observations of the individual patients, and population level empirical evidence, are discussed.

### PACS codes:

87.10.+e (Biological and Medical physics: General theory and mathematical aspects)  
02.30.Zz (Inverse problems)  
02.50.Tt (Inference Methods)  
87.19.Uv (Properties of higher Organisms: Haemodynamics, Pneumodynamics)

# 1. INTRODUCTION

## A. Motivation

The amount of quantitative data available to the clinician at the bedside has grown tremendously due to advances in medical monitoring and imaging technology. This situation is particularly evident in the critical care setting, where patients are monitored and treatments are titrated on a minute-to-minute basis. The limit of the currently available methodologies' capability to assimilate this flood of data into the diagnostic and therapeutic process seems to have been reached. This is evidenced by the fact that an improved capacity to acquire quantitative measurements that convey information highly relevant for therapeutic decision making has failed to improve outcome [1,2]. The difficulty in translating richer data streams into improved clinical outcomes may be partly due to insufficient therapeutic options. We contend, however, that this failure may also be ascribed to the human care providers' limited ability to integrate the sheer volume of available data and to quantitatively interpret the complicated and often nonlinear interactions of the various physiologic subsystems that contribute to these observations [3]. Additionally, the current evidence-based medicine paradigm requires that therapeutic strategies be proven effective in prospective, randomized, controlled clinical trials. Such trials typically use as the basis for randomization a crude segregation of patients into relatively homogeneous subgroups, so that statistically significant differences in outcome between therapies and among subgroups are identified. This approach seems particularly paradoxical in critical care, in view of the massive volume of data available on individual patients, and of the resulting potential to provide truly individualized care [4-6]. This incongruence has clearly hampered more rapid progress in the care of the critically ill.

## B. Traditional approaches to computer-supported decision making in medicine

The potential of computer-based, algorithmic support for medical decision making in data rich environments, and in particular in the context of evidence-based practice, was recognized early on and has been pursued extensively [3,7,8]. Few of these efforts, which mostly have consisted of rule-based expert systems, statistical models, or approaches driven by machine learning ideas such as dynamic bayesian or artificial neural networks, have reached the maturity or level of usefulness to be accepted into the day-to-day practice of critical care medicine [8-10]. These tools either attempt to formalize empirical knowledge already available to a physician (expert systems) or to capitalize on statistical *associations* of phenomena and *inherent structures* of the available dataset. All largely fail to make direct and quantitative use of known causalities and dynamics in the physiologic systems underlying the observed pathophysiology, which are typically characterized by basic science investigations.

A promising approach to incorporating this knowledge into the medical decision making process would be to use mathematical models of physiologic mechanisms to map clinical observations to quantitative hypotheses about physiologic conditions, leading to improved insight into current patient status and, eventually, predictions about responses to therapeutic interventions. While complex quantitative mathematical models of (patho-) physiology abound [11,12], their translation to clinically useful tools has proved challenging. Early examples of applying mathematical models of physiological mechanisms to quantify “hidden” parameters based on clinical measurements include the pioneering work of Bergman in the late 1970s [13], in which an ordinary differential equation model of glucose control was used to quantify insulin sensitivity based on the results of standardized stimulation tests. More recent work in

the same field has focused on accurately quantifying the uncertainty arising in the resulting parameter estimation problems using current methodology, such as Markov-Chain-Monte-Carlo approaches [14]. In the cardiovascular field, which is somewhat more central to critical care, some extremely simple models have been in use for decades and are implemented in commercially available products, examples being the electric circuit analog of the systemic circulation serving to calculate total peripheral resistance, which can then become a therapeutic target, or pulse contour analysis, which performs a model based assessment of systemic flow from arterial pressure waveforms and is still the subject of current research [15,16]. The clinical application of mathematical models of physiology to date has failed to extend to models of sufficient complexity to significantly help alleviate the previously discussed problem of information overload in the diagnostic process.

### **C. Obstacles in applying complex mathematical models in a clinical setting: the inverse problem**

We contend that a key obstacle preventing the successful clinical use of available mathematical models has been the lack of a robust solution to the inverse problem. Since any physiologically reasonable mathematical model of components of the human body will typically be nonlinear and have a large number of parameters, the resulting inverse problem, i.e., inferring parameters and state variables from measured data, will usually be ill-posed in the sense of Hadamard, that is, not admit a unique solution that depends continuously on the data [17]. In addition to the uncertainty resulting from the fundamental ill-posedness of the inverse problem, measurement error and model stochasticity introduce additional sources of uncertainty that affect both forward and inverse problems (Fig. 1).

The most popular approaches to tackling the inverse problem assume the existence of a unique “best” solution, typically by looking for a maximum likelihood estimate by minimizing the sum of squared residuals. More recently, increasing attention has been paid to the quantification of the uncertainty of parameter estimates, using for example the Markov-Chain-Monte-Carlo method [14]. Despite considerable theoretical work and efforts devoted to the development of such algorithms, it seems unsurprising that their utility has been limited to the simplest settings (e.g., [18]).

#### **D. A proposed solution**

We hypothesize that the ill-posedness of the inverse problem reflects clinical reality in the sense that an experienced physician is rarely certain about a patient’s status, despite the large number of available observations. More typically, the physician entertains an evolving differential diagnosis, a list of hypotheses of varying likelihoods about the physiological mechanisms underlying available observations, updated and ranked according to current observations.

We approach the inverse problem in such a way that uncertainty from all sources is quantitatively reflected by the solution, which will consequently take the form of a (typically multimodal) probability distribution on parameter and state space. To achieve this, we combine a mechanistic model of physiologic processes with Bayesian inference techniques to infer posterior probability distributions on parameter and state space from prior (population level and individual) knowledge and quantitative observations. The model itself, along with the inference techniques used, are presented in section 2 of this paper. In section 3, we provide a proof-of-concept implementation to illustrate the potential power of this approach. Finally, in section 4, we discuss implications of this

work as well as future challenges, and possible resolutions, to scaling this approach to realistic settings.

**Table I. Glossary of variables and parameters of the cardiovascular model.**

Symbol	Description	Unit
$f_{HR}$	Heart rate, i.e., the number of complete cardiac cycles per unit time	Hz
$T_{Sys}, T_{Dia}$	Duration of systole (ejection period of cardiac cycle) and diastole (filling part of the cardiac cycle), thus $f_{HR} = \frac{1}{T_{Sys} + T_{Dia}}$	S
$W_S$	Stroke work, the work performed by the heart muscle during cardiac cycle/ejection period	mmHg ml
$I_{CO}$	Cardiac output, total flow generated by the heart per unit time	ml/s
$V_S$	Stroke volume, the volume of blood ejected during 1 cardiac cycle/ejection period	ml
$V_{ES}, V_{ED}$	End-systolic volume, i.e. the ventricular volume at the end of the ejection period, and end-diastolic volume, i.e. the ventricular volume at the end of the filling period	ml
$V_{ED_0}, P_{0_{LV}}, k_E$	Constants characterizing the passive empirical ventricular pressure/volume relationship	ml, mmHg, ml <sup>-1</sup>
$R_{valve}$	Hydraulic resistance opposing ventricular filling. The valve dynamics imposes unidirectional flow.	mmHg s / ml
$P_{ED}$	End-diastolic pressure, i.e. the intraventricular pressure at the end of the filling period	mmHg
$\bar{P}$	Average ventricular pressure during ejection phase	mmHg
$P_{LV}, P_a, P_v$	Pressure in ventricular, arterial, venous compartment	mmHg
$V_{LV}, V_a, V_v$	Volume of ventricular, arterial, venous compartment	ml
$V_{a_0}, V_{v_0}$	Arterial, venous unstressed volume, i.e. volume at which the pressure induced by wall tension is 0 mmHg	ml
$R_{TPR}$	Total peripheral/systemic vascular hydraulic resistance, i.e., the hydraulic resistance opposing the flow through the capillary streambed that is driven by the arterio-venous pressure difference	mmHg s / ml
$I_C$	Flow through capillary streambed, i.e. from arterial to venous compartment	ml/s
$C_{PRSW}$	Preload recruitable stroke work, a contractility index describing by how much the stroke work increases with increases in diastolic filling, quantified through end-diastolic volume	mmHg
$C_a, C_v$	Compliance of arterial, venous compartment	ml/mmHg

$\tau_{Baro}$	Time constant of the baroreflex response, i.e., of the linear low pass characteristic of the physiological negative feedback loop controlling arterial pressure	S
$P_{a_{set}}$	Set point of the baroreflex feedback loop	mmHg
$k_{width}$	Constant determining the shape and maximal slope of the logistic baroreflex nonlinearity	mmHg <sup>-1</sup>

---

## 2. METHODS

### A. A simplified mathematical model of the cardiovascular system and its regulation

The model we developed was designed to be computationally and conceptually simple while achieving a good qualitative reproduction of system responses to alterations in contractility and hydration status. It consists of a continuous representation of the monoventricular heart as a pump, connected to a Windkessel model of the systemic circulation in which arterial pressure is controlled by baroreflex ([19], Fig. 2). The pulmonary circulation is excluded for simplicity, since the perturbations to be studied in our example are not directly related to it. The physiological variables and parameters used in the following exposition are summarized in Table I.

#### 1. The heart as a pump

We developed an ordinary differential equation model of the monoventricular heart by considering a single cycle representation of the emptying (ejection) and filling of the ventricle. The model of ejection was based on the experimentally observed linearity of the relationship between preload recruitable stroke work and end-diastolic volume over a wide range of volumes [20]. This linear relation takes the form:

$$C_{PRSW} = \frac{W_S}{V_{ED} - V_{ED_0}} \quad (\text{Preload recruitable stroke work}) . \quad (1)$$

Simplifying approximate stroke work as pure volume work yields:

$$W_S = \int_{V_{ED}}^{V_{ES}} P(V)dV \approx V_S (\bar{P} - P_{ED}) \quad (\text{Stroke work}) \quad (2)$$

Substitution of (2) into (1) provides an expression for stroke volume.

$$V_S = \frac{c_{PRSW} (V_{ED} - V_{ED_0})}{\bar{P} - P_{ED}} \quad (3)$$

Ventricular filling, on the other hand, is modeled as a simple passive filling through a linear inflow resistance driven by the pressure difference between central veins and ventricle, through the ordinary differential equation (ODE)

$$\frac{dV_{LV}}{dt} = \frac{P_{CVP} - P_{LV}(V_{LV})}{R_{valve}}. \quad (4)$$

In (4), the dependence of ventricular pressure on ventricular volume is governed by the experimentally characterized exponential relationship:

$$P_{LV}(V_{LV}) = P_{0LV} (e^{k_{ELV}(V_{LV} - V_{ED_0})} - 1), \quad (5)$$

yielding

$$\frac{dV_{LV}}{dt} = \frac{P_{CVP} - P_{0LV} (e^{k_{ELV}(V_{LV} - V_{ED_0})} - 1)}{R_{valve}}. \quad (6)$$

Under the assumption of constant filling pressure  $P_{CVP}$ , the ODE (6) is of the general form

$$\frac{dV}{dt} = k_1 e^{k_2 V} + k_3, \quad (7)$$

with constants

$$\begin{aligned}
k_1 &= -\frac{P_{0LV}}{R_{valve}} e^{-k_{ELV} V_{ED0}} \\
k_2 &= k_{ELV} \quad , \\
k_3 &= \frac{P_{CVP} + P_{0LV}}{R_{valve}}
\end{aligned} \tag{8}$$

which resolves to

$$V(t) = k_3(t + C) - \frac{1}{k_2} \ln \left( \frac{1 - k_1 e^{k_2 k_3(t+C)}}{k_3} \right) \tag{9}$$

by quadrature. By letting  $t = 0$  at the beginning of diastole, using end-systolic volume  $V_{ES}$  as the initial condition, and substituting the constants from (8), we determine from (9) the remaining unknown constant uniquely as

$$C = \frac{R_{valve}}{P_{CVP} + P_{0LV}} \left( V_{ES} - \frac{1}{k_{ELV}} \ln \left( \frac{P_{0LV} (1 - e^{k_{ELV} (V_{ES} - V_{ED0})}) + P_{CVP}}{R_{valve}} \right) \right). \tag{10}$$

At a given heart rate  $f_{HR}$ , and assuming an approximately constant duration of systole  $T_{Sys}$  (physiologically, the duration of diastole is much more strongly affected by alterations in heart rate than the duration of systole [21]), the end-diastolic volume will therefore be

$$V_{ED} = V(f_{HR}^{-1} - T_{Sys}), \tag{11}$$

with  $V(t)$  given by (9).

Equation (11) provide a relation between  $V_{ES}$  and  $V_{ED}$ , since  $V(t)$  depends on  $V_{ES}$  through the constant in (10). A second relation is given directly by the fact that

$$V_{ES} = V_{ED} - V_S. \tag{12}$$

Viewing  $V_{ES}$  as a function  $\tilde{V}_{ES}(V_{ED})$  of the end-diastolic volume of the previous beat, and  $V_{ED}$  as a function  $\tilde{V}_{ED}(V_{ES})$  of the end-systolic volume of the previous beat, respectively, we can thus define a discrete dynamical system describing the beat-to-beat evolution of  $V_{ED}$  (or, similarly,  $V_{ES}$ ). Specifically, given the current end-diastolic volume  $V_{ED}^n$ , we can use (3) and (12) to compute  $V_{ES}^n = \tilde{V}_{ES}(V_{ED}^n)$  and use (9), (10), and (11) to obtain  $\tilde{V}_{ED}(V_{ES}^n)$ . Together, these steps yield

$$V_{ED}^{n+1} = \tilde{V}_{ED}(V_{ES}^n) = \tilde{V}_{ED}(\tilde{V}_{ES}(V_{ED}^n)). \quad (13)$$

To obtain a continuous dynamical system amenable to coupling with continuous representations of the physiologic control loops and simulation with available ODE software over long time intervals, we converted  $V_{ES}$  and  $V_{ED}$  to state variables of a continuous time system. This was done by setting their rates of change to the average rates of change over an entire cardiac cycle that would occur during one iteration of the discrete time system for the current  $V_{ES}$  and  $V_{ED}$  values, to obtain

$$\begin{aligned} \frac{dV_{ES}}{dt} &= (\tilde{V}_{ES}(V_{ED}) - V_{ES}) f_{HR} \\ \frac{dV_{ED}}{dt} &= (\tilde{V}_{ED}(V_{ES}) - V_{ED}) f_{HR} \end{aligned} \quad (14)$$

The discrete system (13) and the continuous system (14) share identical sets of fixed points. Indeed, fixed points of the discrete system (13) are given by

$$V_{ED} = \tilde{V}_{ED}(\tilde{V}_{ES}(V_{ED})), \quad (15)$$

and by applying  $\tilde{V}_{ES}$  to equation (15), we have

$$V_{ES} = \tilde{V}_{ES}(V_{ED}) = \tilde{V}_{ES}(\tilde{V}_{ED}(\tilde{V}_{ES}(V_{ED}))) = \tilde{V}_{ES}(V_{ED}),$$

thus  $\frac{dV_{ES}}{dt} = \frac{dV_{ED}}{dt} = 0$  at fixed points of the discrete system. Conversely, inspection shows that fixed points of (14) satisfy (15) and hence are fixed points of (13) as well. Consistent with the dynamics of (13), solutions to the complete circulation model (described below) incorporating the continuous time system (14) very quickly settle to a unique fixed point (Fig. 3).

## 2. The systemic circulation

The circulation is represented by a simple Windkessel model, consisting of linear compliances representing large arterial and venous vessels of the systemic circulation with respective pressures

$$P_\alpha = \frac{V_\alpha - V_{\alpha_0}}{C_\alpha} \quad (16)$$

where  $\alpha = a, v$ . The arterial and venous compartments are connected through a linear resistor representing the total peripheral resistance regulating arterio-venous capillary blood flow,

$$I_C = \frac{P_a - P_v}{R_{TPR}} \quad (17)$$

To simulate the action of the cardiac valves, which do not allow for retrograde flow, the veno-arterial flow generated by the heart was set to

$$I_{CO} = f_{HR} \max(0, V_{ED} - V_{ES}). \quad (18)$$

Assuming conservation of volume at the nodes, the evolution of arterial and venous volumes are thus described by the following differential equations:

$$\begin{aligned} \frac{dV_a}{dt} &= I_C - I_{CO} \\ \frac{dV_v}{dt} &= -\frac{dV_a}{dt} + I_{external} \end{aligned} \quad (19)$$

where  $I_{external}$  represents a possible external blood withdrawal or fluid infusion to or from the venous compartment.

### 3. Baroreflex control of blood pressure

Baroreflex control of blood pressure is implemented based on the established representation of the central processing component of the baroreceptor sensor input as a combination of a sigmoidal nonlinearity (logistic function, in our case) with a linear system [22,23]. For simplicity, we reduced baroreflex activity to a single activating (sympathetic) output instead of the more physiologically accurate balance of stimulating (sympathetic) and inhibiting (parasympathetic) outputs. Since our model of the heart is designed to represent time scales significantly larger than a single beat, the linear part of the baroreflex feedback loop is simplified to display first order low pass characteristics with a time constant on the order of the slowest actuator response (unstressed venous volume control). Pure delays associated with the neural transmission of baroreflex signals are neglected. Specifically, the temporal evolution of the stimulating output from baroreflex central processing is governed by the differential equation

$$\frac{dS}{dt} = \frac{1}{\tau_{Baro}} \left( 1 - \frac{1}{1 + e^{-k_{width}(P_a - P_{a_{set}})}} - S \right). \quad (20)$$

The stimulating output  $S(t)$  of the feedback loop acts on heart rate, total peripheral resistance, myocardial contractility (PRSW), and unstressed venous volume effectors/actuators to adjust blood pressure according to its current deviation from the set point, based on the linear transformation

$$\alpha(t) = S(t)(\alpha_{max} - \alpha_{min}) + \alpha_{min} \quad (21)$$

where  $\alpha = f_{HR}, R_{TPR}$ , or  $c_{PRSW}$ , and

$$V_{v_0}(t) = (1 - S(t))(V_{v_{0\max}} - V_{v_{0\min}}) + V_{v_{0\min}}, \quad (22)$$

since the venous capacitance vessels contract, reducing their unstressed volume, in response to drops in blood pressure.

The combined system of the 5 coupled ODEs (14), (19), and (20) was solved numerically in the MATLAB™ (The MathWorks, Inc., Natick, MA) environment.

#### 4. Parameter selection

The parameter selection process was based on fitting to literature data supplemented by physiologically reasonable assumptions and is fully described in the Appendix. It should be emphasized that our objective was to obtain a reasonably simple, biologically plausible model that describes certain phenomena of interest in a qualitatively correct fashion.

### B. The inference procedure

#### 1. Notation

To allow for a concise description of the procedure applied, we will use the notational conventions described in Table II.

**Table II. Notational conventions for the description of the inference procedure.**

Notation	Description
$x \in X \subset \mathbb{R}^n$	Element of $n$ -dimensional initial condition/parameter space
$y \in Y \subset \mathbb{R}^m$	Element of $m$ -dimensional observation space $Y$
$M : X \rightarrow Y, x \mapsto M(x)$	Deterministic model generating observation vector from known parameters and initial condition
$f_{\Sigma} : \Sigma \rightarrow \mathbb{R}, \Sigma = X, Y$	Joint probability density function on parameter/initial condition space or observation space
$f_{\Sigma}(\beta   \alpha) : \mathbb{P} \times \Sigma \rightarrow \mathbb{R}; \mathbb{P} = X, Y; \Sigma = Y, X$	Conditional probability density function evaluated at $\beta \in \mathbb{P}$ given $\alpha \in \Sigma$

$$g : Y \times Y \rightarrow \mathbb{R}, \quad \text{Measurement characteristic giving probability density of}$$

$$(y, y_{true}) \mapsto g(y, y_{true}) \quad \text{observing } y, \text{ given that the true value of the observable is}$$

$$y_{true}$$


---

For the purpose of this exposition, we are lumping initial conditions and parameters into one product vector space,  $X$ . Additionally, for simplicity, we assume a fully deterministic model that gives a simple mapping from this finite dimensional parameter/initial condition space to a finite dimensional observation space  $Y$  (which may vary depending on the step in the inference procedure). Extending the method to stochastic models is straightforward but computationally more burdensome.

## 2. *Inferring prior densities on the observables*

In a practical application, prior probability densities on parameter/initial condition space would be generated from a finite set of observations of a population, which in itself constitutes an ill-posed inverse problem. For simplicity, we assume a known prior distribution on parameter/initial condition space. To derive a prior probability density on observation space from these assumptions, we calculate

$$f_Y(y) = \int_{\{x \in X | M(x)=y\}} dx f_X(x), \quad (23)$$

using Monte Carlo integration by sampling from the known prior densities on  $X$ , simulating, and estimating  $f_Y$  from the resulting set of simulated observations. To evaluate this density and sample from it, we used the kernel density estimation approach as implemented in the kernel density estimation toolbox for MATLAB [24], using Gaussian kernels and the ‘local’ option for data based selection of kernel bandwidth. This toolbox provides an efficient implementation for the representation of arbitrary multidimensional probability density functions as a sum of kernel functions

with varying standard deviation/bandwidth, and allows for efficient sampling from, and evaluation of, these densities.

### 3. *Inferring posterior densities on the parameters*

The crucial step of inferring posterior densities on parameter/initial condition space from observations and prior probability densities was implemented based on the standard Bayesian calculation

$$f_X(x|y) = \frac{f_Y(y|x)f_X(x)}{f_Y(y)} = \frac{g(y, M(x))f_X(x)}{f_Y(y)}. \quad (24)$$

In equation (24), the prior densities  $f_X(x)$  and  $f_Y(y)$  represent either the initial assumptions on  $X$  (see subsection C below) and  $Y$  (see (23)) or the posteriors of a previous inference step, if sequential observations, possibly with interposed external perturbations (e.g. interventions or diagnostic challenges), are performed. In our implementation, the posterior densities are calculated on a uniform grid, with smoothing applied for the purpose of sampling from these posteriors again, based on a kernel density estimation approach.

### C. **Simulating population variability**

Variability in the simulated population (i.e., in space  $X$ ) was initially restricted to two lumped parameters/states. The characteristics varied were total intravascular volume  $V_{total} = V_a + V_v$ , corresponding to hydration status, and cardiac contractility response range  $[c_{PRSW_{min}}, c_{PRSW_{max}}]$ . Initial conditions for compartmental volumes were generated from  $V_{total}$  by setting them proportional to the unstressed volume of the respective compartment and ensuring that observations were taken only after the system had equilibrated.

Next, we allowed a third lumped parameter, arteriolar responsiveness, which linearly scales the arteriolar resistance range  $[R_{art_{min}}, R_{art_{max}}]$ , to vary. We report the results of this scenario separately to illustrate the effects of higher dimensionality. Two types of prior distributions were examined:

- a) Parameters/initial conditions were assumed to come from independent Gaussian distributions, with means at the selected parameter values (scaling factor of 1) for contractility range (and for arteriolar responsiveness where applicable), and a total intravascular volume that corresponds to a level of sympathetic nervous activity  $S(t) \approx 0.5$  in steady state (Table III). Standard deviations were 0.5 for the scaling factors and 1000 ml for the total intravascular volume. All distributions were truncated at 0 by repeating the sampling if a negative value was drawn.
- b) Parameters/initial conditions were assumed to be distributed uniformly on the intervals ranging 2 standard deviations above and below the means described under a), again truncated at 0.

### 3. RESULTS

#### A. Cardiovascular system simulation

Simulation experiments reveal that the model described by equations (14), (19), and (20) indeed exhibits the desired qualitatively correct behavior, both in its response to alterations in fluid load and contractility (Fig. 4) and in its blood pressure and heart rate responses, on medium to slow time scales, to dynamic challenges such as simulated volume loss (e.g. hemorrhage) and administration (e.g. fluid resuscitation, Fig. 5).

## B. Simulated diagnostic process

To illustrate the probabilistic diagnostic process, we implemented the inference procedure on the cardiovascular model for a set of simplified scenarios. We chose a Gaussian distribution, with varying standard deviation  $\sigma$  and mean  $y_{true}$ , for the measurement characteristic  $g(y, y_{true})$ .

### 1. Single measurement

When only one blood pressure measurement is made, the probable parameter/state range represents a continuum of various combinations of contractility and hydration status. As expected, the high precision measurement ( $\sigma = 10 \text{ mmHg}$ , Fig. 6 and 7, Panel A) leads to more concentrated probability density functions than the low precision measurement ( $\sigma = 30 \text{ mmHg}$ , Fig. 5 and 6, Panel B). This is verified for informative (Gaussian, Fig. 6) and non-informative (uniform, Fig. 7) priors. Two peaks corresponding to the syndromes of “heart failure” (low contractility, normal-high total intravascular volume) and “hypovolemia” (normal contractility, low intravascular volume) can be discerned when blood pressure is measured with high precision for both Gaussian and uniform priors (Fig. 6 and 7, Panel A2). When the measurement is less precise, the peak corresponding to “heart failure” is nearly absent with a Gaussian prior, but not with a uniform prior (Fig. 6 and 7, Panel B2).

### 2. Measurement of response to perturbation

To illustrate the additional diagnostic knowledge gained from perturbing the system, we simulated a fluid challenge [25]. Depending on the system’s response to the administration of 1,500 ml of fluid in the circulation, the updated posterior densities on parameter space are altered significantly (Fig. 6 and 7, Panels A3, A4, B3, B4).

Specifically, the fluid challenge serves to differentiate between cardiac causes of

hypotension (“heart failure”, low contractility, low responsiveness to volume resuscitation, Fig. 6 and 7, Panel A3) and lack of intravascular volume as cause (“hypovolemia”, normal or high contractility, high responsiveness to volume resuscitation, Fig. 6 and 7, Panels A4) for the high precision measurement. With high precision measurements, the failure to restore blood pressure following a fluid challenge virtually eliminates hypovolemia as the cause of hypotension (Fig. 6 and 7, Panel A3), while low accuracy measurements yield an opposite prediction (Fig. 6 and 7, Panel B3), where the most likely cause of hypotension is hypovolemia.

The clinician often wonders whether there is a preferred sequence of diagnostic challenges for ascertaining an accurate diagnosis. We explored this process in a limited fashion by evaluating the commutativity of interventions with respect to diagnostic value. The inference process itself is naturally commutative with respect to the sequence of assimilation of equivalent data (up to errors induced by numerical approximations). Yet, whether the sequence of dynamic interventions delivered to a physiological system for diagnostic or therapeutic purposes is commutative is less clear. We therefore considered the effect of administering two fluid volumes sequentially, either 500 ml then 1000 ml or 1000 ml then 500 ml. After each step, we assimilated blood pressure observations, taking the previous posteriors as the new priors, and we compared the final probability distributions obtained from the two different administration sequences. With parameter sets corresponding to hypovolemia, there was a high degree of commutativity as well as agreement with the posterior density obtained by assimilating a single observation made after a one-time, combined fluid challenge of 1500 ml. In contrast, with parameters corresponding to “heart failure”, there were some differences in the relative weights of the peaks in the posterior densities obtained from the two

different administration sequences, although the qualitative diagnostic inferences implied by these peaks were the same (data not shown).

### 3. *The 3-dimensional setting*

When we allow 3 (lumped) parameters to vary, the structure of the posterior densities becomes much richer. The distributions become truly multimodal, and visualization and interpretation become more challenging. To illustrate this, we have recreated the scenarios from the 2-dimensional experiment. We depict two different visualizations of the grid points accounting for 95% of the total probability mass for the scenarios described earlier (Fig. 8, Panel A and C), as well as for a more ambiguous post-resuscitation observation of 50 mmHg (Fig 8, Panel B). As can be seen, the assimilated observations are still sufficient to meaningfully constrain the probable region in parameter/state space. In both the low (30 mmHg post-resuscitation) and high response (70 mmHg post-resuscitation) scenarios, an additional probability concentration appears. This additional probability mass corresponds to the possibility of shock induced by severely decreased peripheral resistance, which clinically corresponds to a failure of vasomotor tone as observed in septic, anaphylactic, or neurogenic shock states. For intermediate values of the post-resuscitation observation, the structure becomes even richer (Fig. 8, Panel B).

## 4. DISCUSSION AND CONCLUSIONS

### A. Mathematical model of the cardiovascular system

While a greatly simplified physiological representation, our mathematical model (14), (19), (20) of the cardiovascular system fulfills its design objectives: to be qualitatively correct in its response to variations in hydration status and myocardial

contractility while incorporating enough homeostatic mechanisms to make the identification of parameter values underlying observed states realistically ambiguous. The method used to convert the discrete dynamical system representing the sequential filling and emptying of the heart (and the resulting “history awareness” of the system) into a compact system of ordinary differential equations that preserves the physiologic meaning of parameters of the discrete system is, to our knowledge, novel. The model only includes mechanisms that have previously been recognized as important. Cardiovascular simulations achieving these requirements have typically involved either simulating *intra*-beat dynamics, which rapidly becomes computationally prohibitive, or resorting to a beat-to-beat discrete time representation (e.g., [26]). Our model is therefore particularly suited for simulation scenarios where an accurate description of *intra*-beat details is not required, yet a continuous form of *inter*-beat dynamics that preserves parameter meanings is desired.

### **The inference process**

As illustrated by this proof-of-concept implementation, the proposed methodology clearly has the potential to integrate existing mechanistic knowledge and data generated by quantitative measurements in a clinical setting into a tool for assessing patient status. Our approach offers a means to achieve this integration in a way that not only incorporates all available data, but also quantifies the remaining uncertainty, thus avoiding unjustified claims of high certainty that could prove disastrous in a clinical setting. In particular, the clinical concept of differential diagnoses of different likelihoods is reflected in the observed multimodality of posterior probability distributions (Fig. 7, 8, and 9).

In effect, our approach maps clinical syndromes described by a set of observations to configurations of physiologically meaningful pre-observation states and parameters appearing within a mathematical model. Based on the physiological knowledge embodied in the model, certain regions in parameter and state space may in turn be associated with differential diagnoses, similar to the conditions of “hypovolemia”, “heart failure”, and “sepsis” in our simplified example. When this linkage is possible, the quantitative nature of the method presented here allows for the assignment and refinement of probability values to certain diagnoses. This, to our knowledge, is the first time that such a high level concept central to the clinical decision making is shown to emerge naturally from the combination of sequential observations, diagnostic challenges, and physiological principles. Independent of clinical applications, we believe that the methods presented herein open novel avenues of exploring theoretical aspects of clinical epistemology, independent of practical applications.

Since measurement characteristics are described stochastically, the method we demonstrate is not fundamentally limited to assimilating data from device based quantitative measurements, but can also make use of rather qualitative clinical observations such as peripheral perfusion, lung rales or mental status, provided reasonably informative densities on system states or parameters conditional on such observations can be defined. Whether a combination of several subjective (or inaccurate) observations may exploit the physiological coupling of observables and yield informative posterior distributions corresponding, for example, to a carefully performed clinical examination, is a matter of current investigation.

While modifying the order of physiological challenges did not have a tangible impact on diagnostic discrimination in our limited exploration, we anticipate that order

generally matters, as system response to a perturbation can be highly dependent on the system state at the time that the perturbation is delivered. That is, an initial diagnostic challenge will alter the state of the underlying system, which may impact its response to a subsequent challenge. As an extreme example, a lethal and a non-lethal challenge clearly do not commute. Our approach could allow for a theoretical exploration of how to optimize the selection, and order, of diagnostic challenges for maximal information gain in the context of specific clinical scenarios.

There must be congruence between the accuracy of observations and the level of information included in prior distributions. The inappropriate use of informative priors can be misleading in this context. The combination of the informative Gaussian priors with inaccurate observations effectively eliminates the physiologically reasonable “heart failure” peak in both the posteriors after a single observation of low blood pressure and the post-resuscitation posteriors for the low response case, while it is still clearly evident in the case of uniform priors (Fig. 6 and 7, Panels B2 and B3). This example illustrates that a conscious choice needs to be made as to whether an interpretation based on population level probabilities (corresponding to the use of informative priors) or an unbiased assessment of physiological possibilities (corresponding to the use of uniform priors) is more appropriate, when only few low quality measurements are available. Whether an optimal degree of incorporation of population-based information exists, and how such an optimum could be defined, are highly relevant issues that remain to be explored.

## **B. Future Challenges**

There are core theoretical and methodological challenges in expanding the proposed approach to realistic settings. A common aspect of most of these challenges is the “curse

of dimensionality”, associated with the challenge of tackling high dimensional problems in a computationally tractable fashion. Specific sub-problems of immediate interest include the optimal inference of prior densities of parameters and system states from population level data [27], the estimation of posterior densities from prior densities given current observations, the propagation of resulting state densities using estimated parameters, the visualization and computer-aided interpretation of high-dimensional posteriors, the extension of this methodology towards optimization of diagnosis and therapy, perhaps using control theoretical approaches, and finally, the validation of the entire system, or workable subcomponents, according to the criteria of evidence-based medicine. Recent methodological developments in the areas of Markov Chain Monte Carlo methods and sparse grids, as well as the growth of computational power, may contribute to making many of these steps feasible for reasonably sized models and data sets in the near future, possibly even for real-time bedside use.

### **C. Conclusion**

While none of the sub-components of the proposed methodology are entirely novel, we believe that this combined approach provides a conceptually new quantitative framework for a theoretical description of the medical decision making process, which may potentially be harnessed to improve this process. Eventually, this methodology could be extended to an outcome prediction tool, or to a method for the optimization of diagnostic and therapeutic interventions in individual patients. Its practical implementation will clearly require broad interdisciplinary collaborations due to the significant challenges involved. We nevertheless believe that the potential gains in diagnostic effectiveness and efficiency that can be made by taking a quantitative

approach to uncertainty, based on our ever-growing mechanistic knowledge, may make the effort worthwhile.

#### D. Acknowledgements

This work was in part supported under NIH grant R01-HL76157.

### 5. APPENDIX: PARAMETER ASSIGNMENT

The parameters  $P_{0_{LV}} = 2.03$  mmHg,  $V_{ED_0} = 7.14$  ml, and  $k_{E_{LV}} = 0.066$  ml<sup>-1</sup> describing the ventricular pressure-volume relationship were estimated from the experimental data for the left ventricle from [20] using the Levenberg-Marquard non-linear least squares algorithm (Fig. 9).

The remaining parameter values and ranges for variables, as well as the respective sources, are given in Table III (for meaning of parameters, see Table I). When no explicit source is given, assignment was based on the authors' perception of physiologically reasonable values for the simplified system, without claiming quantitative accuracy:

**Table III.** Parameter values for the model of the cardiovascular system and their sources.

Parameter/Variable	Values(s)	Source
$C_{PRSW_{min}}, C_{PRSW_{max}}$	34.5 - 138 erg/ml □ 25.9 - 103.8 mmHg	50 - 200% of average control value from [20], table 1
$R_{valve}$	0.0025 mmHg s/ml	Atrial resistances from [28]
$f_{HR_{min}}, f_{HR_{max}}$	2/3 - 3 Hz	Corresponding to 40 - 180 bpm
$T_{Sys}$	4/15 s	80% of duration of cardiac cycle at max. heart rate, [21], figure 4A
$R_{TPR_{min}}, R_{TPR_{max}}$	0.5335 - 2.134 mmHg s/ml	50%-200% of value used in [29] (1.067)
$V_{a_0}, V_{v_{0min}}, V_{v_{0max}}$	700 ml, 2700 - 3100 ml	Adapted from [29]
$C_a, C_v$	4 ml/mmHg, 111 ml/mmHg	[29]
$P_{a_{set}}$	70 mmHg	
$k_{width}$	0.1838 mmHg <sup>-1</sup>	(corresponding to 99% saturation at 25 mmHg deviation from set point)
$\tau_{Baro}$	20 s	Time constant for control of unstressed venous volume from [28]

## Reference List

1. S. Harvey *et al.*, *Lancet* **366**, 472 (2005).
2. M. R. Shah *et al.*, *JAMA* **294**, 1664 (2005).
3. N. McIntosh, *Clin. Med.* **2**, 349 (2002).
4. A. V. Kulkarni, *Med. Health Care Philos.* **8**, 255 (2005).
5. S. Doherty, *Emerg. Med. Australas.* **17**, 307 (2005).
6. S. R. Sehon and D. E. Stanley, *BMC. Health Serv. Res.* **3**, 14 (2003).
7. J. C. Craig, L. M. Irwig, and M. R. Stockler, *Med. J. Aust.* **174**, 248 (2001).
8. C. W. Hanson, III and B. E. Marshall, *Crit Care Med.* **29**, 427 (2001).
9. C. A. Schurink, P. J. Lucas, I. M. Hoepelman, and M. J. Bonten, *Lancet Infect. Dis.* **5**, 305 (2005).
10. G. Clermont and D. C. Angus, *Ann. Acad. Med. Singapore* **27**, 397 (1998).
11. A. C. Guyton, T. G. Coleman, and H. J. Granger, *Annu. Rev. Physiol* **34**, 13 (1972).
12. S. Zenker, G. Clermont, and M. R. Pinsky, in *Yearbook of Intensive Care and Emergency Medicine 2007 (in press)*, Edited by J. L. Vincent (Springer, 2007).
13. R. N. Bergman, Y. Z. Ider, C. R. Bowden, and C. Cobelli, *Am J. Physiol* **236**, E667-E677 (1979).
14. K. E. Andersen and M. Hojbjerg, *Stat. Med.* **24**, 2381 (2005).
15. B. P. Cholley and D. Payen, *Curr. Opin. Crit Care* **11**, 424 (2005).
16. R. Mukkamala *et al.*, *IEEE Trans. Biomed. Eng* **53**, 459 (2006).
17. J. Hadamard, *Princeton University Bulletin* 49 (1902).
18. K. Hoang, *Toxicol. Lett.* **79**, 99 (1995).
19. O. Frank, *Zeitung für Biologie* **37**, 483 (1899).
20. D. D. Glower *et al.*, *Circulation* **71**, 994 (1985).
21. M. K. Friedberg and N. H. Silverman, *Am J. Cardiol.* **97**, 101 (2006).

22. T. Kawada *et al.*, *Am. J. Physiol Heart Circ. Physiol* **286**, H2272-H2279 (2004).
23. J. V. Ringwood and S. C. Malpas, *Am. J. Physiol Regul. Integr. Comp Physiol* **280**, R1105-R1115 (2001).
24. A. Ihler. Kernel Density Estimation Toolbox for MATLAB  
(<http://www.ics.uci.edu/~ihler/code/kde.shtml>). 2004.  
Ref Type: Computer Program
25. J. L. Vincent and M. H. Weil, *Crit Care Med.* **34**, 1333 (2006).
26. B. J. TenVoorde and R. Kingma, *Stud. Health Technol. Inform.* **71**, 179 (2000).
27. E. T. Jaynes, *Phys. Rev.* **106**, 620 (1957).
28. M. Ursino, *Am. J. Physiol* **275**, H1733-H1747 (1998).
29. M. Ursino, M. Antonucci, and E. Belardinelli, *Am. J. Physiol* **267**, H2531-H2546 (1994).

## FIGURE LEGENDS

**FIG. 1. The forward and inverse problems.** Illustration of the role of a mechanistic mathematical model in linking measurements with abstract quantitative representations of the underlying physiological processes. Respective sources of stochasticity are indicated both for forward/predictive use of the model and inverse/inference type use.

**FIG. 2. Schematic of the simplified model of the cardiovascular system and its control.** Blood is driven from the venous compartment with volume  $V_v$  to the arterial compartment with volume  $V_a$  by the monoventricular heart, which contracts from its end-diastolic volume  $V_{ED}$  to its end-systolic volume  $V_{ES}$ . Reverse flow is prevented by a valve with resistance  $R_{TPR}$ . To complete the systemic circulation, flow from the arterial to the venous compartment has to overcome the total peripheral resistance  $R_{TPR}$ . Baroreflex senses pressure  $P_a$  in the arterial compartment, and it processes the set point deviation through a sigmoidal nonlinearity and a linear element with low-pass characteristics, eventually affecting the actuators  $R_{TPR}$ , unstressed venous volume  $V_{v_0}$ , heart rate  $f_{HR}$ , and myocardial contractility  $c_{PRSW}$ . See text for details.

**FIG. 3. Transient behavior of continuous time cardiac model.** Temporal evolution of actual stroke volume of continuous time system during initial transient of simulation shown in Fig. 5 (solid line) and stroke volume calculated from systolic and end-diastolic volumes that would occur if the discrete dynamical system was advanced

one step from the current values given by the continuous system (dashed). Note that the state of the continuous system rapidly approaches a fixed point of the discrete dynamical system, resulting in superposition of the two curves. The transient is caused by starting integration with a non-equilibrium distribution of fluid between arterial and venous compartments.

**FIG. 4. Starling curves.** Steady state stroke volume with closed baroreflex feedback loop as a function of venous pressure for various contractility factors  $c$  that linearly scale the range of the baroreflex contractility effector branch  $[c_{PRSW_{\min}}, c_{PRSW_{\max}}]$ . Simulations were performed by varying total intravascular volume between 3000 and 8000 ml and plotting stroke volumes vs. venous pressures after 600 s of simulated time.

**FIG. 5. Simulation of fluid withdrawal and reinfusion.** Fluid is drawn from or reinfused into the venous compartment at constant rate. Vertical lines indicate the beginning and end of withdrawal and reinfusion.

**FIG. 6. The diagnostic inference process, informative priors.** (*color online*) Probability densities for high precision (standard deviation 10 mmHg, Panel A) and low precision (standard deviation 30 mmHg, Panel B) measurements of blood pressure for *Gaussian* prior densities. A/B1 show the assumed prior densities, A/B2 show the posterior densities resulting from a single arterial pressure measurement of 25 mmHg, A/B3 show the posterior densities if subsequent to the initial measurement, 1500 ml of fluid are applied intravenously resulting in a pressure measurement of 30 mmHg, while

A/B4 show the posterior densities if the measurement after fluid application is 70 mmHg.

**FIG. 7. The diagnostic inference process, uniform priors.** (*color online*)

Probability densities for high precision (standard deviation 10 mmHg, Panel A) and low precision (standard deviation 30 mmHg, Panel B) measurements of blood pressure for *uniform* prior densities. The panel assignments are analogous to figure 6. Note that the axes are scaled differently due to the narrower support of the (compactly supported) priors used.

**FIG. 8. 3-Dimensional inference.** (*color online*) Posterior probability densities for post-resuscitation observations of 30 mmHg (Panel A), 50 mmHg (Panel B), and 70 mmHg (Panel C) mean arterial blood pressure. The left column depicts densities at grid-points corresponding to 95% of the total probability mass, while the right column depicts the approximate surface enclosing this volume. The origin is in the far bottom corner for all figures. Shadows represent orthogonal projections to the contractility/total intravascular volume plane.

**FIG. 9. Endiastolic pressure-volume relationship.** Least squares fit of the empirical exponential pressure-volume relationship used to determine parameters from the experimental end-diastolic measurements from reference [20], Fig 6, bottom right panel.



## 6. FIGURES

Figure 1.

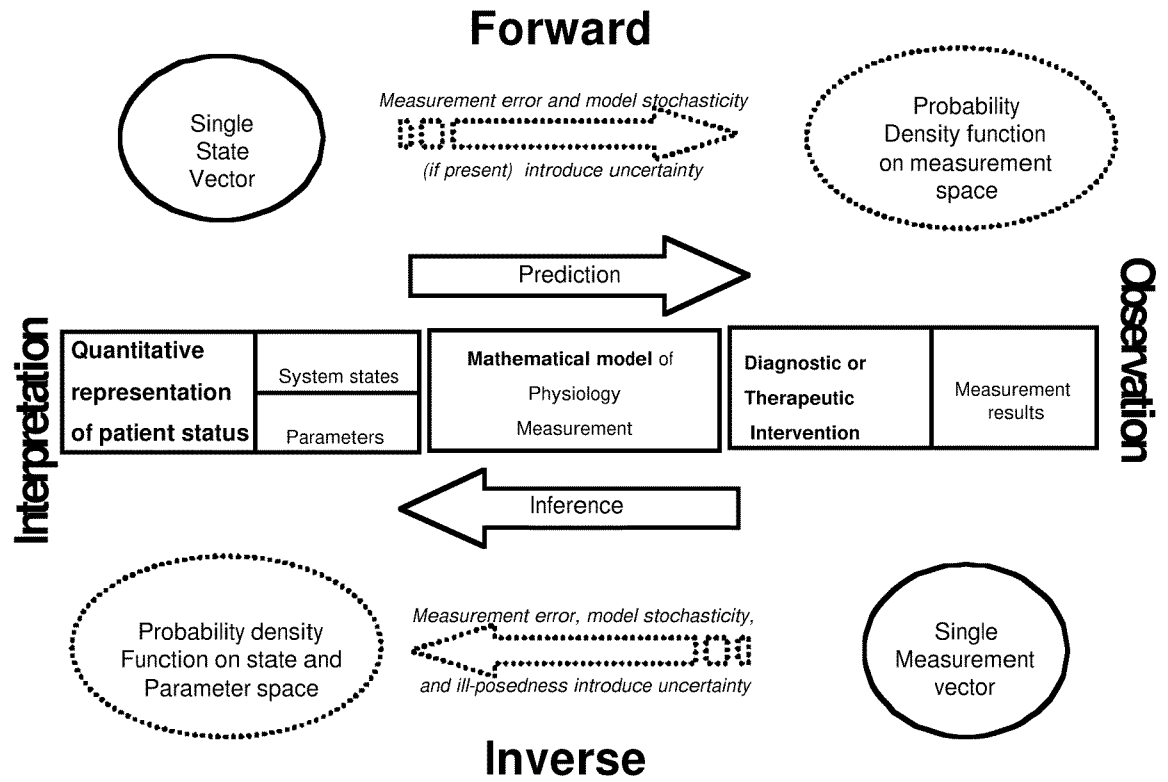


Figure 2.

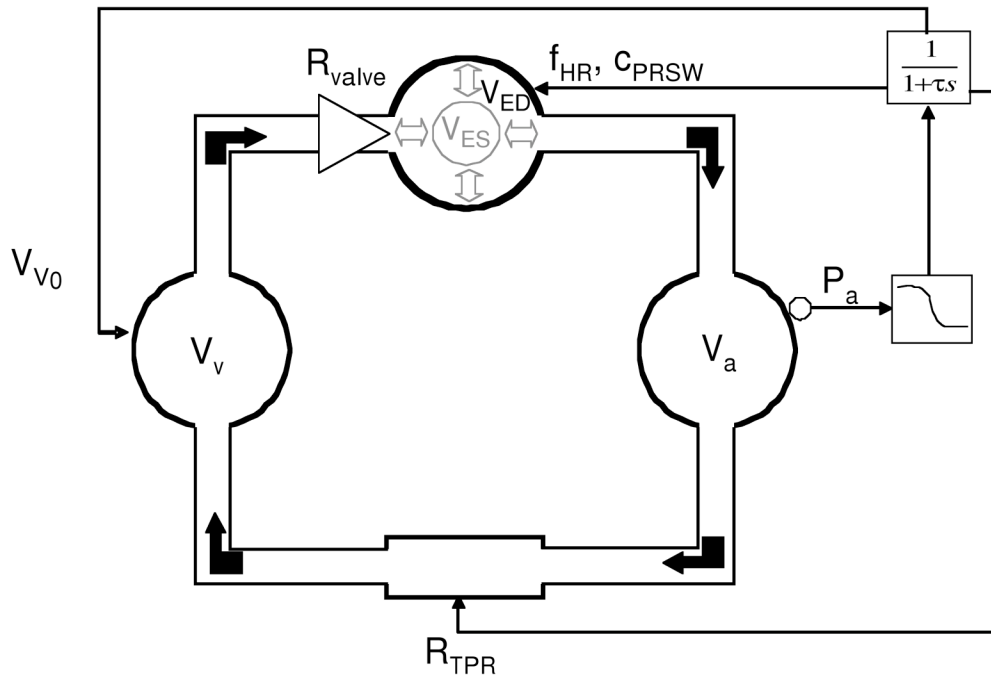


Figure 3.

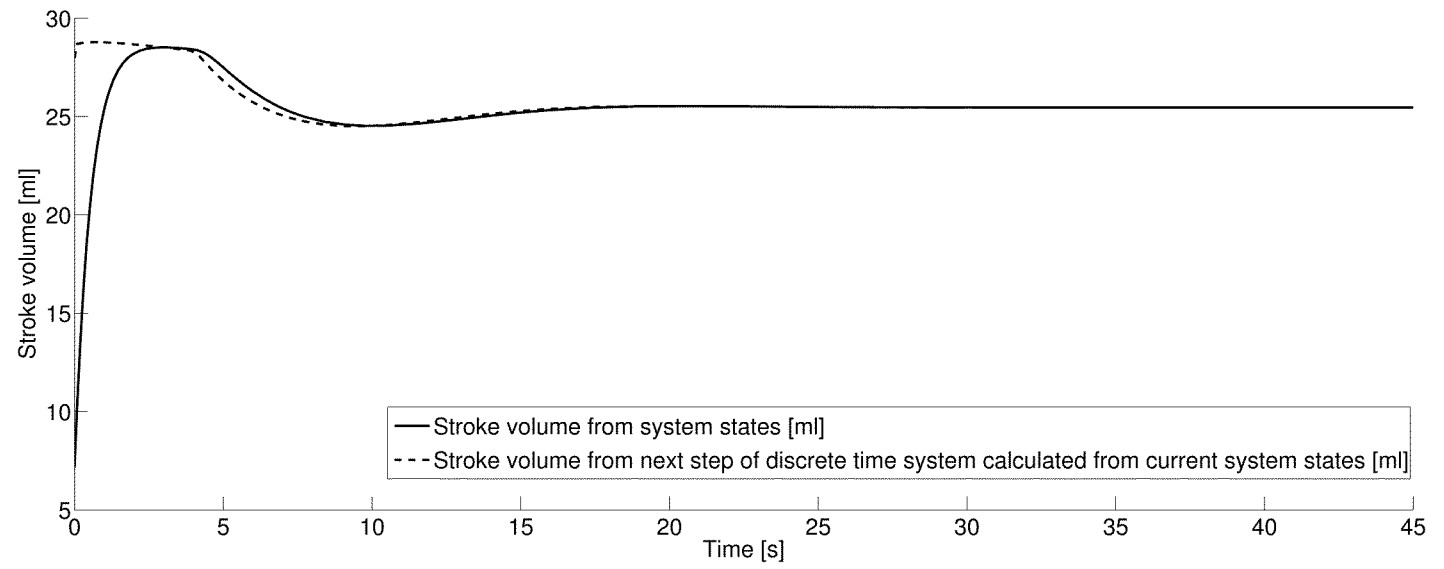


Figure 4.

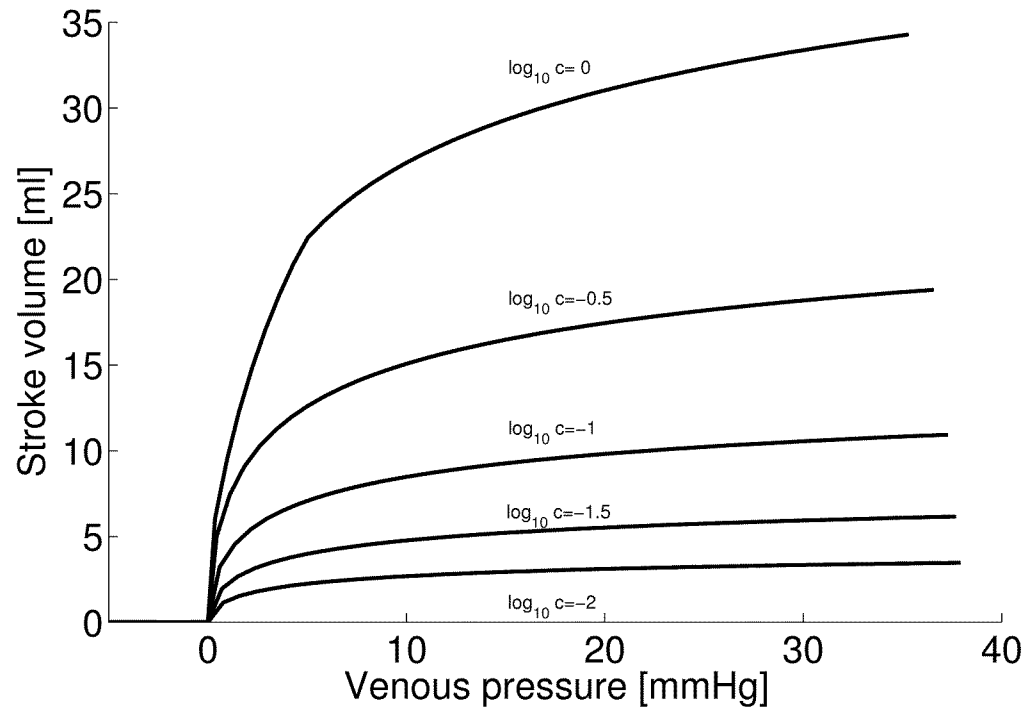


Figure 5.

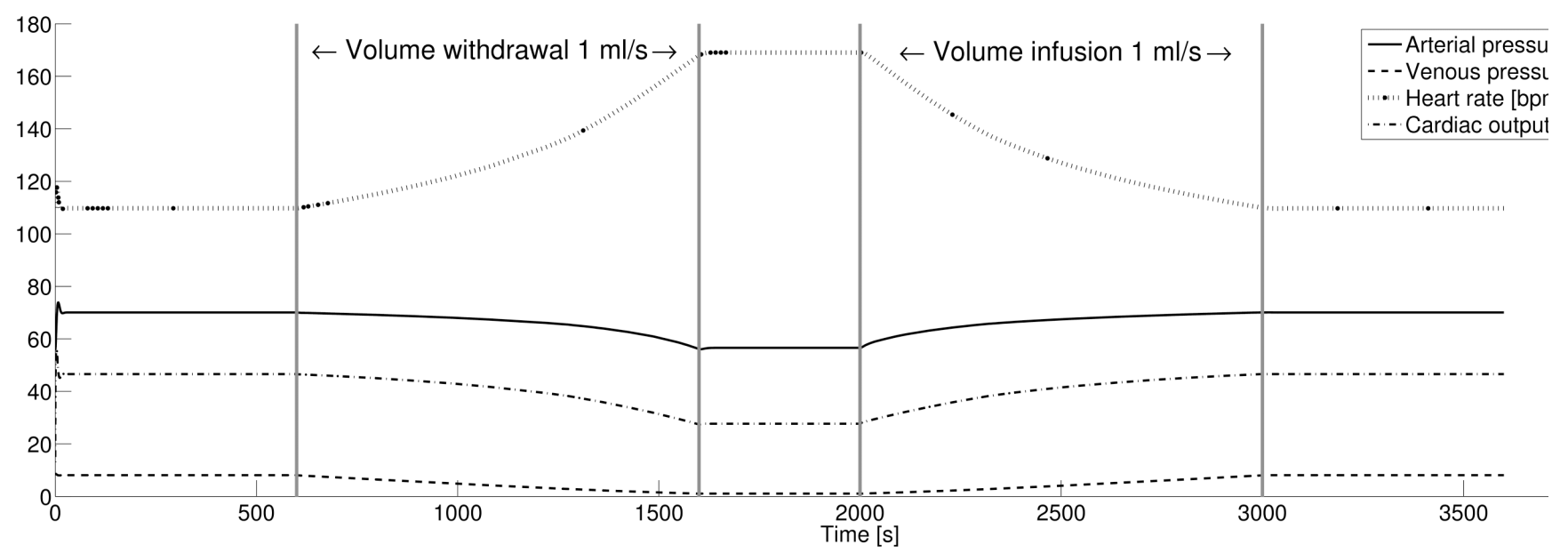


Figure 6.

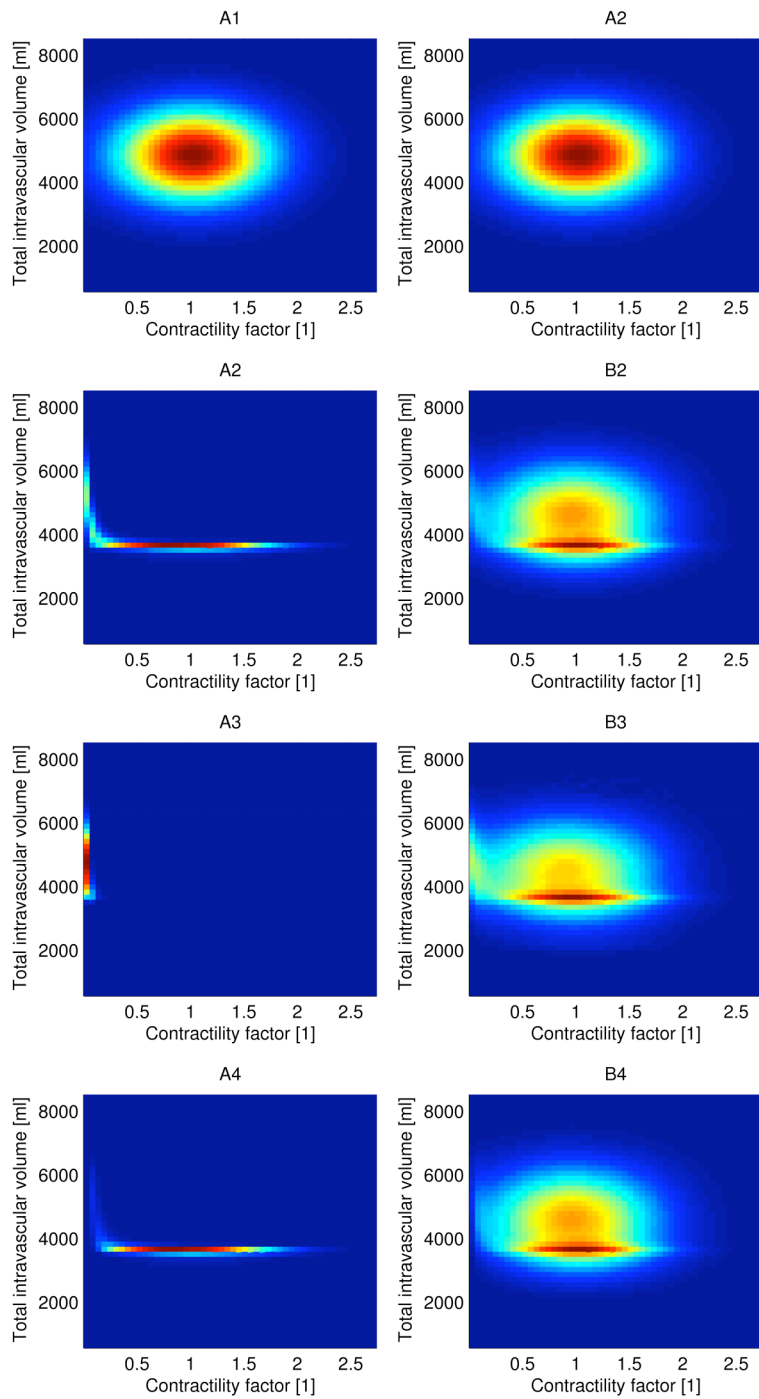


Figure 7.

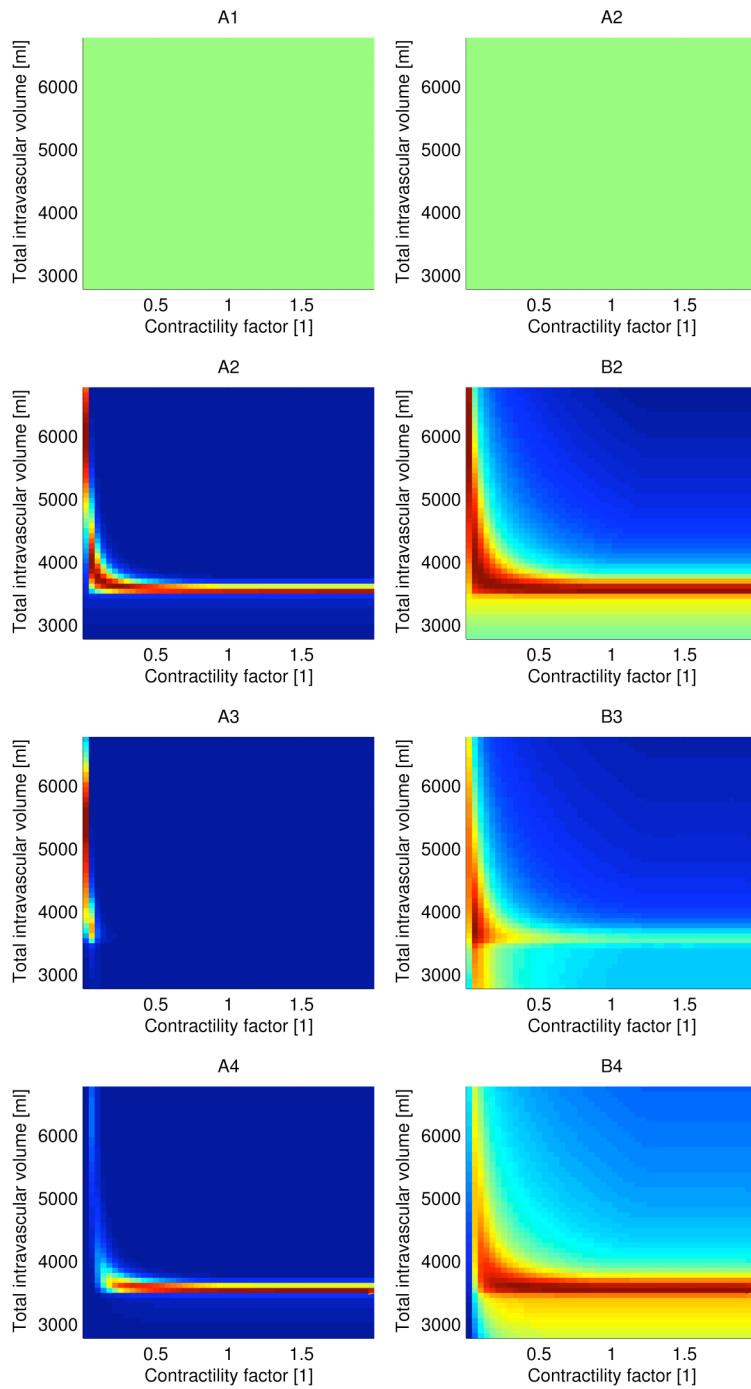


Figure 8.

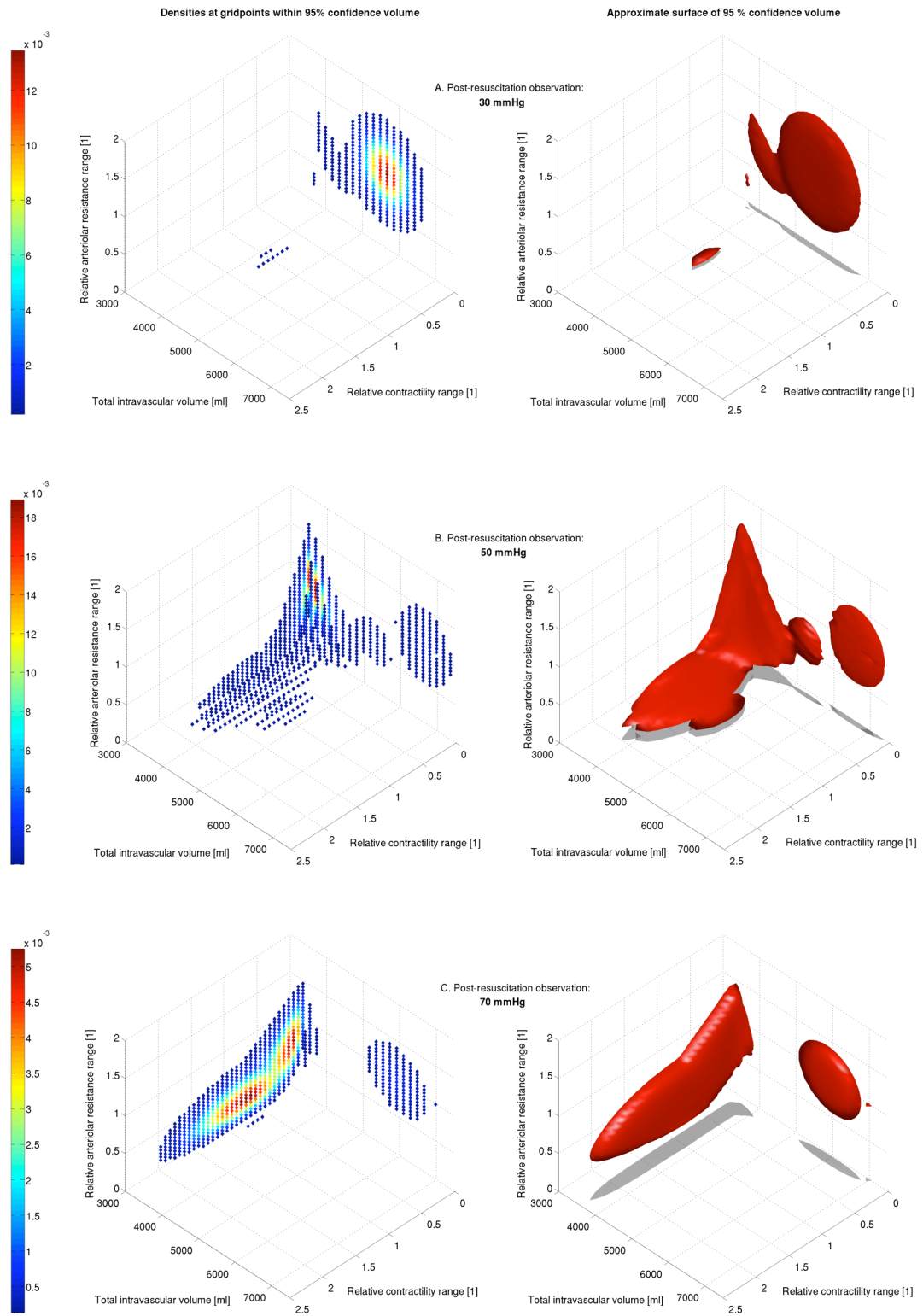


Figure 9.

